Supporting Information

Hammell et al. 10.1073/pnas.0908131106

SI Text

Results. *daf-12* genetic interactions suggest that *daf-12* functions entirely via the modulation of let-7-Fam miRNA expression. If *daf-12* acts entirely through let-7-Fam miRNAs, we would expect *daf-12* to have the same genetic interactions with *lin-28* and *lin-46* as let-7-Fam or miRISC components do. Indeed loss of *lin-46* enhances the retarded phenotype of reduced *daf-12* alleles (Table S1), just as *lin-46*(*0*) enhances the retarded phenotype of let-7-Fam(*0*) mutant animals, or *nhl-2*(*0*) (Table S1) (1). Loss of *lin-28* does not suppress the retarded phenotypes of any of these compound mutant animals (Table S1) (1). The observation that loss of *lin-28* does not affect the retarded phenotype of *lin-46*(*0*)*; daf-12*(*rh61*) mutant larvae is further evidence that the retarded phenotypes of *daf-12*(*rh61*) larvae do not require *lin-28*.

By contrast, when *lin-46* is present, the precocious phenotypes observed in *lin-28*(*0*) larvae are epistatic to the retarded phenotypes of let-7-Fam(*0*) animals (1). Similarly, we find that *lin-28*(*0*) precocious phenotypes are epistatic to the retarded phenotypes observed in either *nhl-2*(*0*), or *nhl-2* (*0*)*; daf-12*(*rh61*) mutant strains. This is despite the observation that the *nhl-2*(*0*)*; daf-12*(*rh61*) double mutant displays a more retarded phenotype than either single mutant. (Table S1). Because *lin-28*(*0*) can suppress this strongly retarded strain, but cannot suppress the retarded phenotype of any compound mutants that possess the *lin-46*(*0*) mutation, this suggests that *daf-12* functions in the same genetic pathway as *nhl-2* and the let-7-fam miRNAs and in parallel to activities of *lin-46* and *lin-28*.

Finally, the simultaneous reduction of *nhl-2*, *lin-46*, and *daf-12* activities produces a striking retarded heterochronic phenotype, where triple-mutant animals reiterate L2-specific seam cell division patterns at all subsequent molts (Fig. S3). These phenotypes are due to the overexpression of *hbl-1* because *hbl-1*(*RNAi*) completely suppressed these phenotypes (Fig. S3).

Materials and Methods. For the dafachronic acid assays, (25S),26–3-keto-4-cholestenoic acid (dafachronic acid) was kindly provided by David Mangelsdorf (University of Texas Southwestern, Dallas). Dafachronic acid was added to 20 μL of 6× concentrated OP50 bacteria and seeded onto freshly poured 2-mL NGM plates (lacking peptone and carrying 30 μg/mL streptomycin to inhibit bacterial growth; this ensures the same amount of food on each plate) to make the appropriate final concentration of dafachronic acid per plate. After 1 h, gravid adult hermaphrodites of the strains AA199 *daf-9*(*dh6*)*; dhEx24[daf-9+, sur-5::GFP]*, VT1911 *mir-241*(*n4316*)*; daf-9*(*dh6*) *mir-84*(*n4037*)*; dhEx24*, or VT2033 *mir-48 mir-241*(*nDf51*)*; daf-9*(*dh6*) *mir-84*(*n4037*)*; dhEx24* were added to the plates and allowed to lay ≈100 eggs and were then removed. GFP-positive animals were removed 2–3 days later. For dauer formation assays, plates were incubated at 20 °C for 3 days. Because partial and transient dauers were often observed, similar to what is observed in *daf-12*-ligand-binding-domain mutants (2), larvae were mounted onto slides and observed by Nomarski optics. Because we were interested in the decision to form dauer and not the ability of complete dauer differentiation to occur, larvae with dauer alae anywhere along the length of the body were scored as dauer larvae. For Mig assays, larvae were incubated at 20 °C for 3–5 days, and Mig was scored in L4 or adult hermaphrodites under the dissecting microscope.

Analysis of TaqMan Data from Staged Animals. For comparisons of wild-type with *daf-12* mutant larvae, embryos were selected by hypochlorite treatment, followed by hatching overnight in the absence of food. Synchronized L1 larvae were then grown at 20 °C on NGM plates with sufficient OP50 bacteria to prevent crowding until most of them were in the L2 molt (as assessed by developmental landmarks such as gonad development and lack of pharyngeal pumping), at which time they were harvested. Two independent biological replicates were prepared in this manner for each strain. For comparisons of wild-type larvae in different environmental conditions, the same procedure was followed, except that embryos were plated immediately after hypochlorite treatment without subjecting larvae to starvation. Larvae grown in "sparse" conditions were plated at low density on standard NGM plates seeded with OP50. "Crowded" plates contained both a crude preparation of dauer pheromone (3) and streptomycin to inhibit bacterial growth. Larvae on "crowded" plates entered L2d because they all had a darkened appearance because of increased fat storage, and they spent more time in L2 than larvae on "sparse" plates. At the concentration of pheromone used, L2d larvae grown in parallel formed dauer larvae at a frequency of >50% (two biological replicates) or not at all (one biological replicate). Crowded and sparse plates were grown side by side at 20 °C until most of them were within L2 or L2d as assessed by the extent of gonad development, at which time they were harvested. RNA was prepared by using TRIzol (Invitrogen) reagent, and multiplex TaqMan assays were carried out according to the instructions of the manufacturer by using an ABI 7900HT Fast-Real Time PCR System (Applied Biosystems).

For each biological replicate, mean and standard deviation of the raw Ct value was calculated from the three technical replicates. miRNAs with mean Ct values ≥30 were eliminated from analysis because some miRNA knockout mutants can show Ct values >30 (X.K. and V.A., unpublished), demonstrating the inability of this assay to distinguish real signal from background at these values. Any miRNA that was poorly measured (if the standard deviation of the Ct value from the technical replicates was ≥1 Ct) was also removed. The remaining mean Ct values for mutant strains were plotted against those of wild type (for comparisons with *daf-12* mutants, see Fig. S1) or against sparse conditions (for comparisons between different environmental conditions). Linear regression was used to determine a calibration line for the mutant versus wild-type Ct values as a function of Ct. This calibration line would account for small differences in the amount of total RNA input from the mutant versus wild-type strains, ultimately giving a relative expression level for each miRNA in the mutant versus wild type. Any global affect on miRNA levels would not be apparent from this analysis. From the equation for the calibration line, the distance of each point (miRNA) from the line was calculated and used as ΔCt. To establish an estimate for the scatter of all points from the calibration line, we then calculated the mean distance of all points (removing the five points furthest from the line and the five points closest to the line so as not to bias this scatter estimate in either direction). Subtracting this mean calibration scatter from the individual distances gives a conservative estimate of ΔΔCt, and the fold change was calculated as $2^{\Delta\Delta Ct}$ multiplied by either +1 or −1 depending on whether the mean Ct for that miRNA was above or below the calibration line. To obtain the mean fold change for all biological replicates, the average was taken between the

calculated fold change for each individual replicate. The mean estimated noise was calculated as follows. For the mean estimated noise in the ΔΔCt values, $\sigma(\Delta\Delta Ct)$, we used the formula $\sqrt{[(stdev_{wt})^2 + (stdev_{mut})^2 + (stdev_{mean\ distance\ from\ line})^2]}/3]$. The mean estimated noise on the fold change was calculated by using Min-Max errors, because a simple root mean square distance calculation cannot be used for errors on an exponential variable. Specifically, we first calculated the average of $2^{(-\Delta\Delta Ct+\sigma(\Delta\Delta Ct))} - 2^{-\Delta\Delta Ct}$ and $2^{-\Delta\Delta Ct} - 2^{(-\Delta\Delta Ct-\sigma(\Delta\Delta Ct))}$ (called ''average-noise'') for each biological replicate, then used the formula $\sqrt{[(average\text{-}noise_{biological\ replicate\ 1})^2 + (average\text{-}noise_{biological\ replicate\ 2})^2 + average\text{-}noise_{biologicalreplicate3})^2}/3]$. Significance was assessed by using Z-scores where $Z = [(mean\ fold\ change) - 1]/stdev_{meanfoldchangeofallmiRNAs}$, where the mean fold change of all miRNAs excluded the five greatest and the five smallest fold change values. A miRNA was deemed to be significantly changed if its fold change had a Z-score ≥ 2.32 ($P \leq 0.01$) and if there was $\geq$2-fold change in two or more biological replicates. Data in Table 1 are displayed as (mean fold change) ± (mean estimated noise).

1. Abbott AL, et al. (2005) The let-7 microRNA family members mir-48, mir-84, and mir-241 function together to regulate developmental timing in *Caenorhabditis elegans*. *Dev Cell* 9:403–414.
2. Antebi A, Culotti JG, Hedgecock EM (1998) daf-12 regulates developmental age and the dauer alternative in *Caenorhabditis elegans*. *Development* 125:1191–1205.
3. Vowels JJ, Thomas JH (1994) Multiple chemosensory defects in daf-11 and daf-21 mutants of *Caenorhabditis elegans*. *Genetics* 138:303–316.

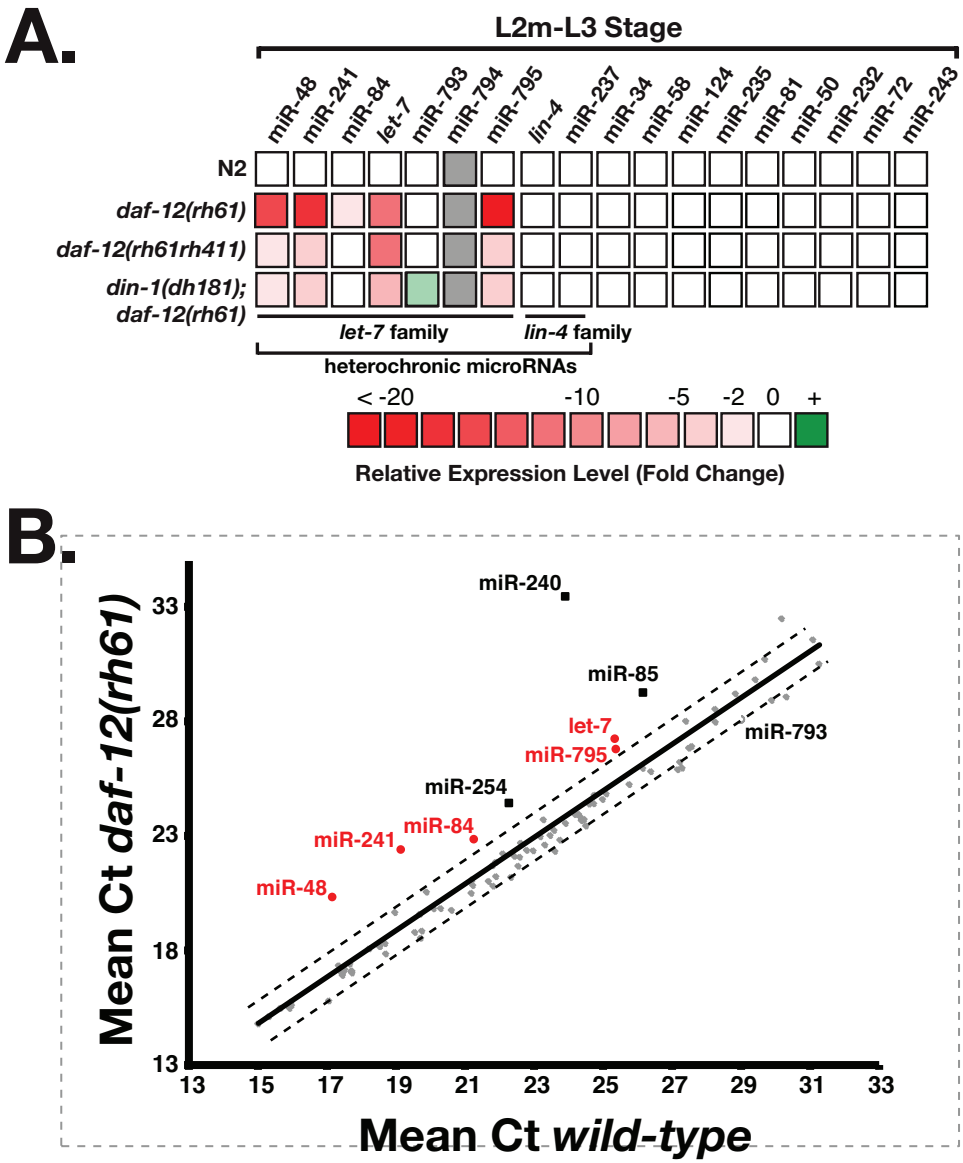

Fig. S1. *daf-12* regulates levels of let-7-Family miRNAs both positively and negatively. Results of mir-TaqMan assays to quantify levels of mature miRNAs (see *Materials and Methods*). (*A*) Heat map showing levels of let-7-Family miRNAs in *daf-12* mutant backgrounds. For comparison, *lin-4*-family and a few other miRNAs are also shown. (*B*) Raw Ct data from one biological replicate, comparing wild-type miRNA expression levels with those derived from similarly staged *daf-12*(*rh61*) animals. The mean Ct of three technical replicates from wild-type larvae was plotted against that of *daf-12*(*rh61*). Because the levels of most miRNAs were unchanged, these miRNAs form a line with a slope near 1. Only a few miRNAs are clear outliers, including let-7-family miRNAs (red); these outliers are beyond the limits of statistical significance ($P < 0.01$) in this sample (represented by dashed lines).

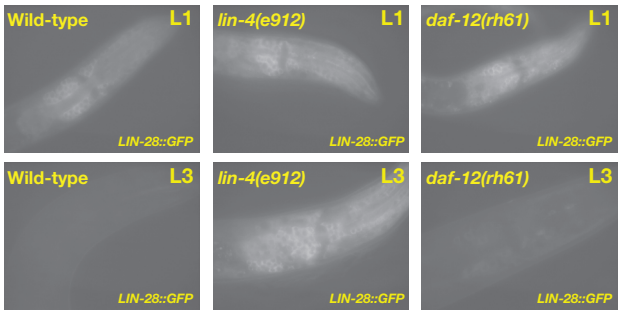

Fig. S2. LIN-28::GFP requires *lin-4* for its normal down-regulation whereas LIN-28::GFP is normally down-regulated in *daf-12(rh61)* mutants.

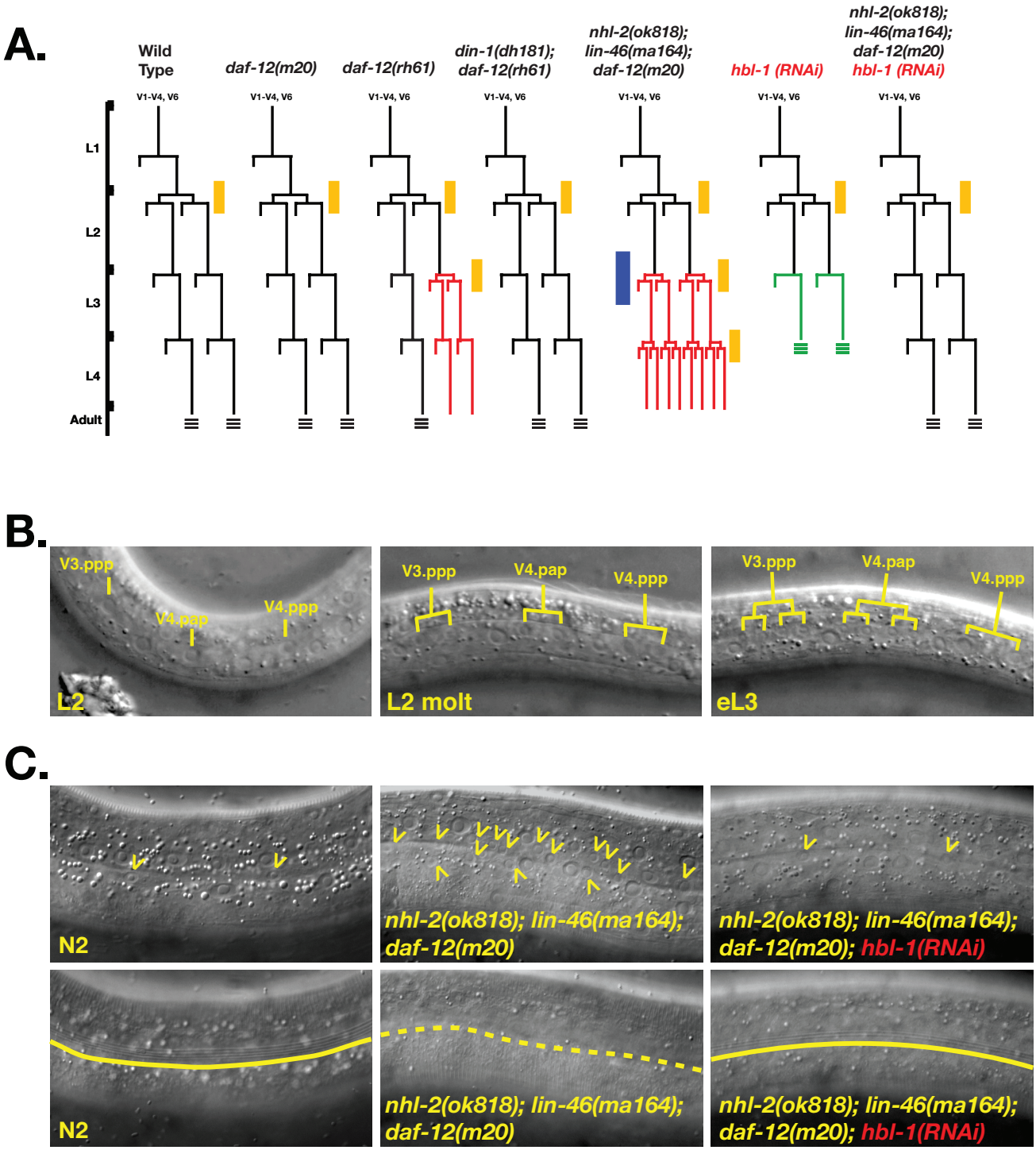

Fig. S3. *daf-12* functions in parallel to *lin-46* and in concert with *nhl-2* to inhibit L2 cell fate specification. (*A*) Seam cell lineage diagrams illustrating the heterochronic phenotypes of various mutant strains analyzed in Table S1. Orange bars indicate the L2-specific seam cell division program. Lineages of cells that express retarded heterochronic phenotypes are drawn in red. The blue bar indicates the time interval of lineage analysis of *nhl-2; lin-46; daf-12* mutants in *B*. (*B*) L2-specific seam cell division programs are reiterated at the L3 stage in *nhl-2*(*ok818*)*; lin-46*(*ma164*)*; daf-12*(*m20*) mutants. (*C*) RNAi of *hbl-1* suppresses theheterochronic phenotypes of *nhl-2*, *lin-46*, and *daf-12* compound mutants.

Table S1. Genetic interactions between *daf-12* and other genes that regulate L2 to L3 cell fate specification

			Percentage of animals with adult alae syntheses*							
			Alae at the L3 molt				Alae at the L4 molt			
	Strain	Genotype	Absent	Gap	Comp	*n*	Absent	Gap	Comp	*n*
1	N2	Wild type	100	0	0	26	0	0	100	26
2	VT1363	*nhl-2*(*ok818*)	100	0	0	28	0	4	96	26
3	VT739	*lin-46*(*ma164*)†	100	0	0	26	0	4	96	27
4	DR20	*daf-12*(*m20*)	—	—	—	—	0	0	100	31
5	VT1943	*daf-12*(*rh411rh61*)	—	—	—	—	0	0	100	45
6	VT1390	*daf-12*(*rh61*)	100	0	0	22	0	100	0	28
7	VT1333	*nhl-2*(*ok818*); *lin-46*(*ma164*)	100	0	0	21	12	88	0	26
8	VT1394	*nhl-2*(*ok818*); *daf-12*(*m20*)	—	—	—	—	0	96	4	25
9	VT1457	*nhl-2*(*ok818*); *daf-12*(*rh61*)	—	—	—	—	46	54	0	24
10	VT938	*lin-46*(*ma164*); *daf-12*(*m20*)	—	—	—	—	0	96	4	26
11	VT1687	*lin-46*(*ma164*); *daf-12*(*rh61*)†‡	—	—	—	—	83	17	0	24
12	VT1395	*nhl-2*(*ok818*); *lin-46*(*ma164*); *daf-12*(*m20*)	—	—	—	—	93	7	0	28
13	VT517	*lin-28*(*n719*)	0	0	100	24	—	—	—	—
14	VT937	*lin-28*(*n719*); *lin-46*(*ma164*)	100	0	0	22	0	0	100	25
15	VT1424	*lin-28*(*n719*); *nhl-2*(*ok818*)	0	6	94	34	—	—	—	—
16	VT1527	*lin-28*(*n719*); *daf-12*(*rh61*)§	0	11	89	28	—	—	—	—
17	VT1370	*lin-28*(*n719*), *nhl-2*(*ok818*); *lin-46*(*ma164*)	100	0	0	20	19	81	0	21
18	VT1572	*lin-28*(*n719*), *nhl-2*(*ok818*); *daf-12*(*rh61*)§	0	15	85	20	—	—	—	—
19	VT1577	*lin-28*(*n719*); *lin-46*(*ma164*); *daf-12*(*rh61*)†§	100	0	0	21	100	0	0	20
20	RG559	*hbl-1*(*ve18*)	0	35	65	20	0	59	41	22
21	VT1426	*lin-46*(*ma164*); *hbl-1*(*ve18*)	82	11	7	27	0	42	58	26
22	VT1463	*nhl-2*(*ok818*); *hbl-1*(*ve18*)	54	31	15	26	0	37	63	27
23	VT1377	*nhl-2*(*ok818*); *lin-46*(*ma164*); *hbl-1*(*ve18*)	93	7	0	27	0	33	67	27
24	VT1936	*cgh-1*(*ok492*)¶	—	—	—	—	0	2	98	41
25	VT1960	*cgh-1*(*ok492*), *daf-12*(*rh411rh61*)¶	—	—	—	—	0	68	32	28

*Presence and quality of cuticular alae structures were assayed by Nomarski DIC optics. Only one side of each animals was scored.
†Animals contain *unc-76*(*e911*) linked to *lin-46*(*ma164*). The *unc-76*(*e911*) mutation does not affect heterochronic gene expression.
‡Animals were derived from a parental strain containing an *szT1*(*I;X*) chromosome that balances *daf-12*(*rh61*).
§Animals were derived from a parental strain containing an *szT1 lin-28*(*n719*) chromosome(X:I) which balances *daf-12*(*rh61*).
¶Animals were derived from segregants of parental animals containing an hT2(I:II) chromosome that balances cgh-1(ok492).